Whorl-Like Collagen Fiber Arrangement Around Emissary Canals in the Posterior Sclera

Hongshuang Lu,[1] Yijin Wu,[1] Jianping Xiong,[1] Nan Zhou,[1] Masahiro Yamanari,[2] Michiaki Okamoto,[2] Keigo Sugisawa,[1] Hiroyuki Takahashi,[1] Changyu Chen,[1] Yining Wang,[1] Ziye Wang,[1] and Kyoko Ohno-Matsui[1]

[1]Department of Ophthalmology and Visual Science, Institute of Science Tokyo, Tokyo, Japan
[2]Tomey Corporation, Nagoya, Aichi-ken, Japan

Correspondence: Kyoko Ohno-Matsui, Department of Ophthalmology and Visual Science, Institute of Science Tokyo, 1-5-45 Yushima, Bunkyo-ku, Tokyo 1138510, Japan; k.ohno.oph@tmd.ac.jp.

Received: January 17, 2025
Accepted: February 21, 2025
Published: March 18, 2025

Citation: Lu H, Wu Y, Xiong J, et al. Whorl-like collagen fiber arrangement around emissary canals in the posterior sclera. *Invest Ophthalmol Vis Sci.* 2025;66(3):35. https://doi.org/10.1167/iovs.66.3.35

Purpose. To investigate the collagen fiber arrangement around emissary canals in the posterior sclera.

Methods. One hundred sixty-five eyes of 93 patients who underwent polarization-sensitive optical coherence tomography (PS-OCT) examinations in 2019 in the Institute of Science Tokyo were studied. Multimodal imaging, including streamline images derived from PS-OCT data, B-scan images, and indocyanine green angiography (ICGA) images, was used to investigate the collagen fiber arrangement around emissary canals and scleral pits in vivo. Additionally, the collagen fiber arrangement around the emissary canals in porcine sclera was examined using scanning electron microscopy and light microscopy.

Results. Streamline images showed whorl-like collagen fiber arrangements on all eyes, and 25 eyes were selected for the analysis. All whorls corresponded to emissary canals on B-scan images. The whorls were confirmed to correspond to the posterior ciliary artery entries in three eyes and posterior vortex vein exits in three eyes with available ICGA images. Streamline cutaway images showed that the whorls surrounded the emissary canals throughout the entire course. In 16 eyes with 20 scleral pits, whorls were seen surrounding all the pits. Microscopic study using porcine sclera confirmed the whorl-like structures around the emissary canals ex vivo and demonstrated tangentially arranged collagen fiber bundles forming the circle.

Conclusions. The collagen fibers are arranged as whorl-like structures around the vessel emissary canals in the posterior sclera, which is a knowledge gap for basic scleral histology. Additionally, this study demonstrated a strong correlation between PS-OCT findings and microscopic histology, underscoring PS-OCT's utility in detecting scleral collagen fiber arrangements.

Keywords: polarization-sensitive optical coherence tomography, scleral collagen fiber, emissary canals

The sclera, forming the outer coat of the eye, is a fibrous connective tissue composed of dense bundles of collagen, a few elastic fibers, fibroblasts, and a moderate amount of amorphous ground substance, such as proteoglycans and glycoproteins.[1–3] The scleral collagen fibers are considered to be crucial in determining the biomechanical behavior of the eye, playing a critical role in maintaining the shape of the eye and protecting the eye from mechanical insults.

There are areas of discontinuity of the posterior sclera. The largest foramen is the optic nerve head (ONH) canal, which allows the passage of the optic nerve and central retinal artery and vein. In addition, there are 15 to 20 emissary canals where perforating scleral vessels (PSVs) penetrate the sclera, including posterior ciliary arteries (PCAs)[4] and posterior vortex veins (VVs).[5,6] These areas with discontinuous sclera are considered structurally vulnerable against mechanical insults especially in highly myopic eyes involving an increase of axial length and significant thinning of the sclera. Previous studies, both in vivo[7–9] and ex vivo,[10,11] have documented a circumferential collagen fiber arrangement around the ONH canal,[7–11] which are believed to provide biomechanical support to the lamina cribrosa, and to the nerves and vessels that pass through it.[12] For the emissary canals, however, the scleral collagen fiber arrangements have not been thoroughly investigated.

Polarization-sensitive optical coherence tomography (PS-OCT) is a functionally extended OCT device. Unlike conventional OCT devices, which are limited to assessing the thickness and the curvature of the sclera, PS-OCT can obtain additional information on the tissue that alters the polarization state of the light. One of the optical properties that can be measured by PS-OCT is birefringence, an optical property exhibited by tissues like smooth muscles and collagen fibers, where the medium has varying refractive indices based on the state of polarized light.[13] The optic axis of

a birefringent medium is the direction where light waves propagate at a consistent velocity, regardless of polarization. Birefringent media generally have multiple optic axes, with the "slow axis" (higher refractive index) aligning with the long axis of biological fibers. Thus PS-OCT can determine collagen fiber orientation by measuring these axes. This technique is widely used to study ocular structures, including the cornea, retinal nerve fiber layer, and sclera.[8,14–17] In the posterior segment, the attenuation of signal penetration by the thick choroid often prevents the full thickness of normal sclera from being visualized in vivo, and highly myopic eyes, with substantially thinner choroid and sclera, are ideal for analyzing scleral structure in vivo using PS-OCT.

During our preliminary study of the posterior sclera with PS-OCT in highly myopic patients, we observed whorl-like collagen fiber arrangements that we suspected to be associated with the emissary canals of the PSVs. The primary aim of this study was to verify this hypothesis and to explore the potential structural and functional roles that these arrangements may play within the scleral matrix. To achieve this objective, we first compared multimodal in vivo imaging for highly myopic eyes and then verified the histological configuration under microscopy using porcine eyes ex vivo.

Methods

Subject Enrollment

The study protocol was in strict adherence to the tenets of the Declaration of Helsinki and received approval from the Ethics Committee of Institute of Science Tokyo. We retrospectively analyzed the medical records of 165 eyes of 93 patients who underwent PS-OCT examinations in May and June 2019 at the Advanced Center of High Myopia at the Institute of Science Tokyo. To select cases that would allow optimal analysis of posterior scleral configuration under conditions closely resembling normal physiology, we implemented stringent exclusion criteria, including images with poor quality, such as images affected by media opacities including dense cataracts or vitreous opacity and images compromised by excessive motion or blinking artifacts; eyes with conditions that affect the performance of the segmentation algorithm and signal detection, including but not limited to extensive retinoschisis, myopic neovascularization, tractional detachment of retina, and large intrachoroidal cavitation; eyes with highly irregular scleral shape or highly steep curvature; and significant scleral signal attenuation caused by thick overlying choroid.

During data screening, whorl-like collagen fiber arrangements were observed on all eyes. Because of the stringent exclusion criteria, 25 eyes from 16 patients met the inclusion criteria and were selected for further analysis. All patients were Japanese. The demographic information is shown in the Table.

PS-OCT Examination and Image Processing

In this study, we employed a prototype PS-OCT system (Tomey Co., Nagoya, Japan) using a swept laser at a 1050 nm center wavelength with 100 kHz A-scan rate. The details of this system have been described previously,[18] where the depth-resolved polarization properties are measured without compromising the effective A-scan rate, enabling wide-field imaging of the fundus as well as conventional swept-source OCT. The raw PS-OCT data contained polarization properties of the target in a mathematical form called Jones matrix, which has complex-valued 2×2 matrix at each spatial pixel. The measured data were processed to obtain the optic axis by algorithms developed earlier.[8] The contrast mechanism of birefringent collagen fiber is as follows briefly: when the propagating direction of the light is oblique or perpendicular to the optic axis, which is the case of the fundus imaging, the medium exhibits two different refractive indices that result in alteration of the state of polarization along the axial depth. The orientations of the optic axes projected on the plane perpendicular to the propagating direction of the light are determined mathematically by PS-OCT.[8] Strictly speaking, the above description is for the case of perfectly aligned fibers. In practice, however, the scleral collagen fibers have interwoven structure, which is mostly beyond the resolution of OCT.[19] As a result, we observe net birefringence created by the interwoven fibers, where birefringence of the individual fibers is partially cancelled out. The optic axis of the net birefringence is attributed as preferential orientation, which have been studied using wide-angle X-ray scattering, small-angle light scattering, second harmonic generation microscopy, and polarized light microscopy.[10,11,20] Compared to these techniques, a unique feature of PS-OCT is the depth-resolved measurement in vivo.

Table. Demographic Information of Subjects

Parameter	Subjects for Normal Emissary Canal Analysis (25 Eyes of 16 Patients)	Subjects for Scleral Pits Analysis (16 Eyes of 14 Patients)
Age (years)	57.50 ± 14.16	65.47 ± 8.36
Gender (Number of patients)		
Male	5	5
Female	11	9
Axial length (mm)	29.72 ± 1.26	31.17 ± 1.62
Refractive error (spherical equivalent, diopters)*	−12.83 ± 4.59	−13.42 ± 4.65
Best corrected visual acuity (logMAR unit)	0.13 ± 0.34	0.66 ± 0.62
META-PM classification (Number of eyes)†		
Tessellated fundus	1	0
Diffuse choroidal atrophy	14	0
Patchy choroidal atrophy	5	4
Macular atrophy	5	12

* Eyes with intraocular lenses were excluded from this calculation.
† Grading system of pathologic myopia developed by the Meta-analysis for Pathologic Myopia (META-PM) Study Group.

Investigative Ophthalmology & Visual Science

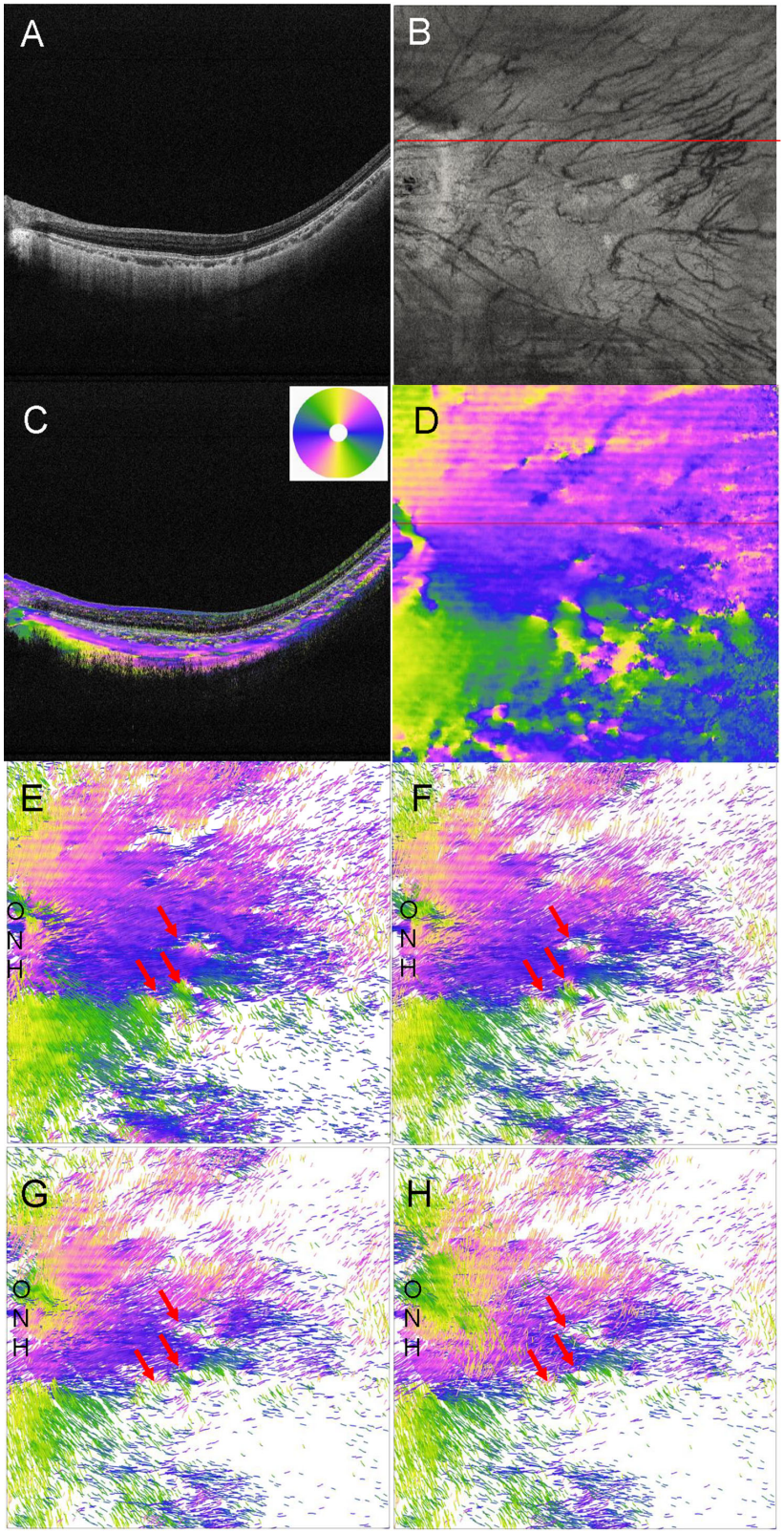

Figure 1. **(A, B)** The B-scan OCT intensity image and en face OCT intensity image at the CSI extracted from polarization-sensitive OCT (PS-OCT) data, respectively. **(C)** The optic axis image with a cyclic colormap to indicate the orientation of local birefringence, where the pixels above thresholds of the signal intensity and local retardation are shown and other pixels are replaced with the gray-scaled intensity. **(D)** The en face optic axis image of the sclera under the CSI with an axial averaging for 15 pixels (67 µm). **(E)** En face streamline image where upper layers of the volumetric data is cropped at the CSI level. **(F)** En face streamline image cropped at the level of 5 pixels (22.35 µm) lower than the CSI. **(G)** En face streamline image cropped at the level of 10 pixels (44.7 µm) lower than the CSI. **(H)** Outside view (i.e., viewing from the outer surface of the sclera). The *red arrows* indicate the whorl-like structures of fiber arrangements, which became increasingly obvious at deeper levels.

Investigative Ophthalmology & Visual Science

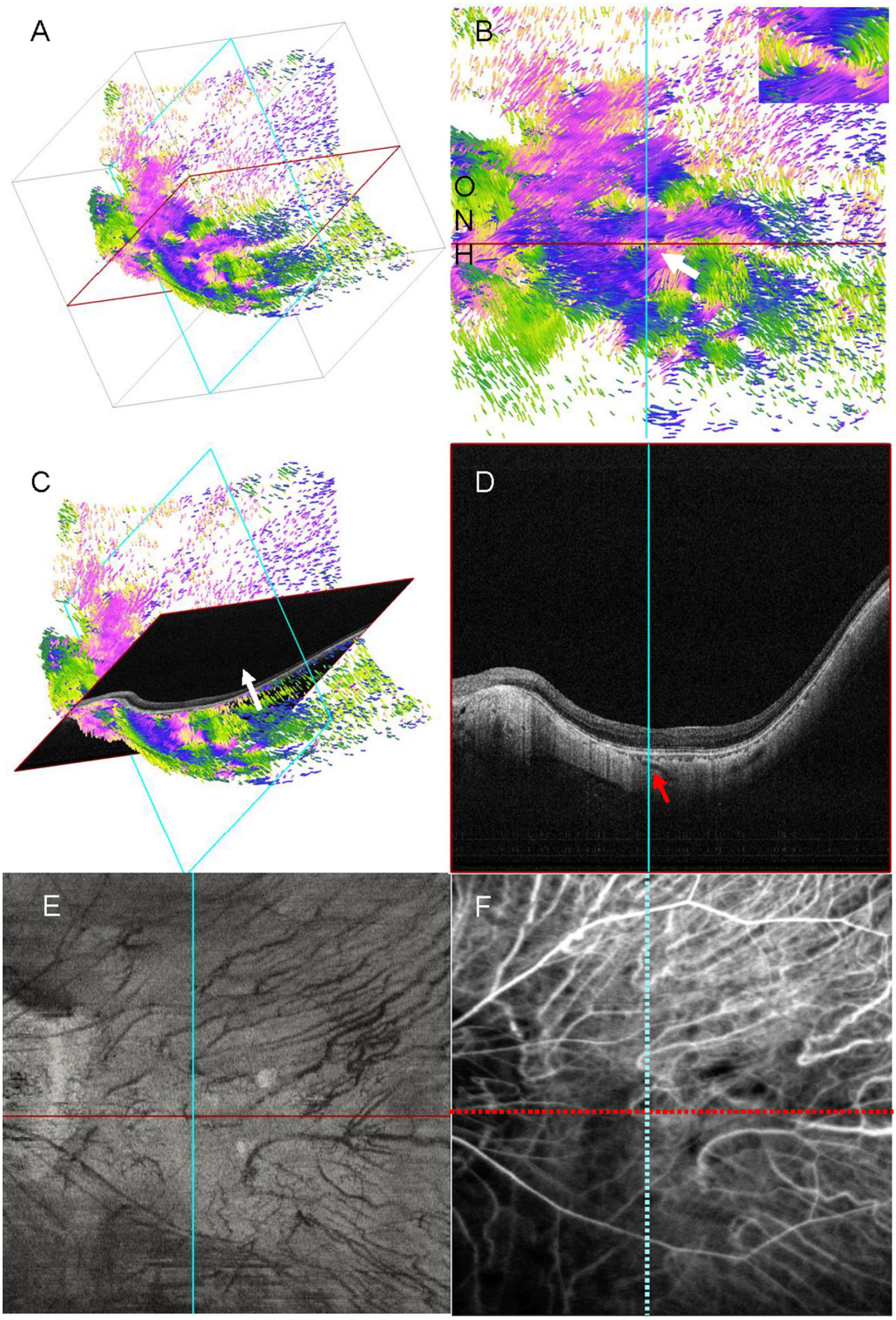

Figure 2. Identification of emissary canals on OCT intensity B-scan images and ICGA images. **(A)** Image showing the three-dimensional (3D) structure of the streamline rendering of the scleral fibers viewed from an oblique camera angle. **(B)** En face view with red and light blue reference lines crossing at the center of the whorl-like fiber arrangement (*white arrow*); A magnified image showing the whorl-like structure at the crossing of the red and blue reference lines is shown on the right upper corner. ONH indicates the optic nerve head. **(C)** Same 3D structure as image **A**, displaying the specific horizontal B-scan corresponding to the *red reference line* in images **A** and **B**. **(D)** OCT intensity B-scan image viewed from the camera angle indicated by the *white arrow* in image **C**. On this image, color rendering of the scleral fibers are hidden, leaving only the B-scan image and the *light blue reference line*, and an vessel emissary canal (*red arrow*) can be seen at the site indicated by the *light blue line*. **(E)** En face OCT intensity image at the CSI showing the location of the center of the whorl-like structure. **(F)** Cropped image of the ICGA arterial phase with horizontal (*red*) and vertical (*light blue*) *dashed lines* to indicate the same entry site of the PCA by referring to retinal vessels and choroidal vessels as the landmarks.

Investigative Ophthalmology & Visual Science

The retinal scans covered an area of 9 × 9 mm^2, centered on the macula, and were acquired using a raster scanning protocol with 1024 × 256 A-scans in the horizontal and vertical directions. The system provided an axial resolution of 7.3 µm and a depth measurement range of 4.49 mm within the tissue. Figures 1A and 1B show the OCT intensity B-scan image and en face OCT intensity image extracted from PS-OCT data, respectively. Figure 1C shows the optic axis image with a cyclic colormap indicating the orientation of net birefringence. Figure 1D shows the en face optic axis image of the sclera under the choroid-sclera interface (CSI) with an axial averaging for 15 pixels (67 µm), where the axial digital resolution of 4.47 µm/pix is smaller than the optical resolution.

Because the optic axis is a vectorial contrast that shows the orientation of the net birefringence created by the fibrous tissues, plotting or rendering methods dedicated to the vectorial data are preferred. Streamline rendering is one of such methods, and it has been used to visualize scleral collagen fibers in previous studies using polarized light microscopy ex vivo[10] and PS-OCT in vivo.[8] In the current study, we used ParaView 5.12.0 (Kitware Inc., New York, NY, USA) for volumetric streamline rendering of the optic axis, and the method was the same as the previous study.[8] Figure 1E shows the streamline image of the optic axis under the CSI.

Throughout the entire thickness of the sclera, the collagen fiber arrangements are not uniform as seen in Figure 1C and reported in previous studies.[10,21] In addition to visualizing the en face streamline image at the level of CSI, we also created cutaway images at different depths from CSI (Figs. 1F–H).

Correspondence of Emissary Canals With Whorl-Like Structures

Figure 2 showed the procedure to investigate the structural relationship between multimodal images at the site of whorl-like collagen fiber arrangements. The volumetric streamline rendering of the optic axis was created by ParaView (Fig. 2A). A horizontal (red) and vertical (blue) reference lines were introduced to pinpoint the center of the whorl-like structures (Fig. 2B). By displaying the horizontal OCT B-scan corresponding to the red reference line (Fig. 2C), the structure of the sclera at the site of the whorl center can be observed on B-scan images, indicated by the blue reference line (Fig. 2D). Characteristic hyporeflective areas indicative of PSVs were observed, as reported by the previous study.[22] The same site can also be pinpointed on the intensity image (Fig. 2E), and the retinal vessel and choroidal vessels were used as landmarks to manually crop the indocyanine green angiography (ICGA) images, and reference lines were manually added on the ICGA images to further verify if the whorl-like structures corresponded to PCA emissaries or posterior VV exits (Fig. 2F).

Collagen Fiber Arrangements Around Scleral Pits at the Site Of PSV Emissaries

As vulnerable points of the sclera, previous studies have identified focal scleral ectasia or scleral pits at the sites of emissary canals within areas of extensive choroidal patchy atrophy.[23,24] To study the collagen fiber arrangements around these particularly fragile sites, we included cases with choroidal patchy atrophy and scleral pits at the sites of PSV emissary canals. Because scleral pits usually occur in cases with severe conditions, the above exclusion criteria did not apply to these cases, and we included all available cases as long as the area of interest was unaffected. In this study, scleral pits were detected in 16 eyes of 14 patients. The demographic information is also shown in the Table.

Basic Clinical Data Collection

The age and gender of patients were collected. All subjects underwent comprehensive ophthalmic examinations. Data included best-corrected visual acuity, refractive error (spherical equivalent), axial length (IOL Master 700; Carl Zeiss Meditec Co., Jena, Germany), and myopic maculopathy according to META-PM classification[25] based on fundus photos were recorded and analyzed. ICGA images were obtained with Heidelberg Spectralis HRA system (Heidelberg Engineering, Heidelberg, Germany). The largest width of the scleral opening on B-scan images at the CSI level was measured using an in-house developed analyzing software (Owl Eye, version 1.6.5; Tomey Co., Nagoya, Japan).

Ex Vivo Verification of the Whorl-Like Structures Using Porcine Eyes

Porcine eyes were obtained from a local slaughterhouse within two hours postmortem. The eyeballs were dissected into scleral eyecups, and a 4 × 4 mm^2 area of the posterior scleral containing the PSVs was excised under a surgical microscope. For hematoxylin and eosin (H&E) staining, the tissue was treated by the following protocol: The tissue was first fixed with 4% paraformaldehyde and stored under 4°C overnight, dehydrated by 30% sucrose, and cryosectioned into 10 µm slices. For scanning electron microscopy (SEM) observation, the scleral tissue was fixed in 2.5% glutaraldehyde in 0.1 M phosphate buffer and stored overnight at 4°C. Because the lamina fusca is relatively loosely connected to the scleral stroma, it can get easily displaced and even detached during the dehydration process. Therefore the lamina fusca together with some superficial scleral layers were removed with a blade, and collagen fiber arrangements within the scleral stroma were observed. The tissue was then post-fixed with 1% osmium tetroxide (OsO_4) in 0.1 M phosphate buffer for two hours. After fixation, the tissue was gradually dehydrated in a graded ethanol series, starting from 50% to 90%, with each concentration applied for 10 minutes. This was followed by three consecutive 10-minute treatments in 100% ethanol. The tissues were then dried using a critical point drying apparatus (HCP-2; Hitachi Ltd., Tokyo, Japan) with liquid CO_2. Finally, the specimen was sputter-coated with platinum before scanning electron microscope (JSM7900F; JEOL, Tokyo, Japan) observation. Cryo-sectioned slides from one eye were also treated with the SEM preparation protocol and observed under SEM.

Results

Comparison of Multimodal Imaging (Streamline Images, B-Scan Intensity Images, and ICGA Images)

The average number of whorl-like structures was 8.9 ± 2.4 per eye on streamline images, ranging from six to 16 (Fig. 3).

Investigative Ophthalmology & Visual Science

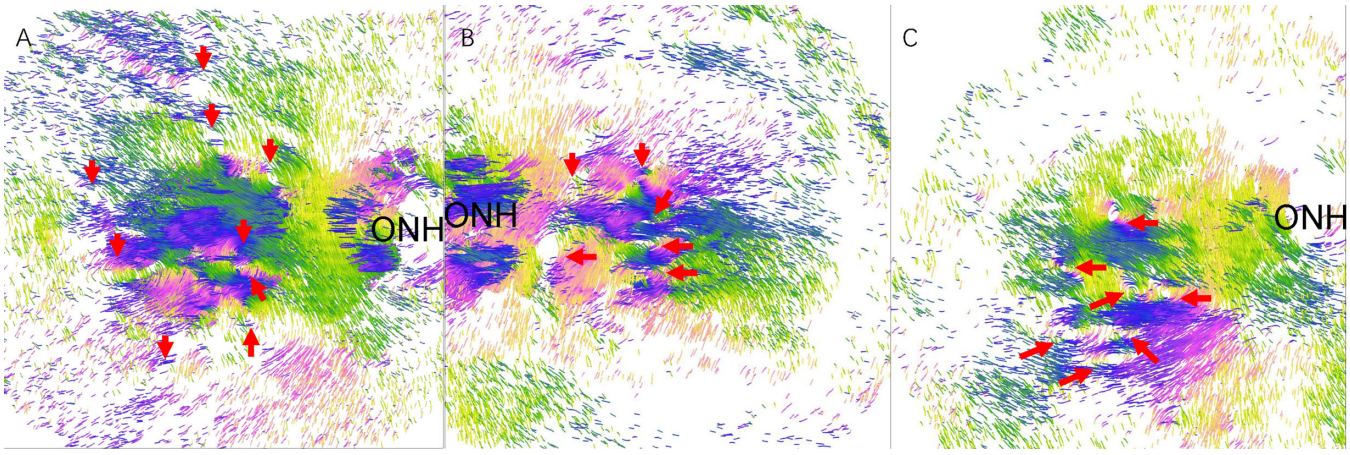

Figure 3. Whorl-like structures (*arrows*) visualized on streamline images of three typical cases viewed from the inside the eye. The streamline images were cropped at 20 pixels (89.4 µm) **(A)**, 20 pixels (89.4 µm) **(B)**, and 10 pixels (44.7 µm) **(C)** from choroid-sclera interface.

These structures were universally verified by B-scan intensity images to correspond to the emissary canals of PSVs (Fig. 4). Additionally, three eyes had arterial phase ICGA images, and all whorl-like structures were confirmed to encircle the PCAs (Fig. 4); in another three eyes with posterior VVs on venous phase ICGA images, exits of all posterior VVs were also observed to be surrounded by whorl-like structures (Fig. 5). The mean largest width measured on B-scan images at the level of CSI was 274.63 ± 189.55 µm (range 70.31 µm to 843.75 µm) for PSV emissary canals.

Whorl-Like Structures Surrounding the Entire Course of the Emissary Canals

Because the scleral emissary canals may follow various courses, including perpendicular, spiral, or oblique,[1] we observed the whorl-like structures at different depths in the sclera along the entire course of the emissary canals (Fig. 6 and Supplementary Video S1). Furthermore, in four eyes, two whorl-like structures observed on the inner side of the streamline image merged into a single larger whorl-like structure on the outer side. This merger was corroborated by B-scan images, which confirmed the convergence of two emissary canals at a deeper level of the sclera (Supplementary Fig. S1).

Whorl-Like Structures Surrounding Scleral Pits at PSV Emissaries

Scleral pits are full-thickness focal scleral excavation around the PSV emissaries in pathologically myopic eyes with extensive choroidal atrophy.[23,24] In the 16 eyes, a total of 20 pits were identified. Whorl-like structures encircled each pit, regardless of their sizes (Fig. 7). The average maximum width of the scleral pits at CSI was 471.68 ± 219.06 µm, ranging from 149.41 µm to 896.48 µm.

Microscopic Examination of Posterior Emissary Canals of Porcine Eyes

SEM and H&E staining images (Figs. 8A–E) vividly illustrated collagen bundles encircling the emissary canals. Under higher magnification, these bundles appear tangentially arranged, forming a distinctive ring around the canals (Fig. 8F). Notably, one or more vessels may share a single emissary canal, and when a single vessel traverses the canal, it often adheres to one side rather than positioning centrally (Fig. 8C). In addition to the vessels, longitudinally aligned collagen fibers are observed along the vessels' path within the emissary canal (Figs. 8C, 8D).

Discussion

In this study, we used PS-OCT to analyze the posterior scleral collagen fiber arrangements in highly myopic eyes, highlighting whorl-like collagen fiber configurations around the emissary canals of PSVs, mainly comprising PCAs and posterior VVs. Furthermore, our study revealed that while scleral collagen fiber arrangements were depth-dependent and exhibited significant differences between the inner and outer layers,[10,21] the whorl-like structures around the emissary canals persisted throughout the entire thickness of the sclera and consistently aligned with the courses of the emissary canals. Even in cases with scleral pits at the emissary canals in eyes with extensive myopic choroidal atrophy, whorl-like structures remained undestroyed. Based on these findings, we hypothesize that the whorl-like structures maintain structural consistency and adaptability under both normal and pathological conditions. However, further investigations, particularly histological studies using microscopy, are necessary to verify this hypothesis across various disease states. Moreover, we examined posterior porcine sclera using H&E staining and SEM and verified the whorl-like structure around the emissary canals ex vivo. Detailed observations using SEM revealed that the whorl-like structures were tangential configuration of collagen bundles encircling the canals. The correspondence between in vivo and ex vivo results demonstrated the reliability of PS-OCT as a valuable tool to provide accurate information on the scleral structure.

Our research distinguishes itself from prior studies using PS-OCT[7,26] by using streamline images, which provide a clearer and more intuitive depiction of the preferential orientation formed by the interwoven collagen fibers in the posterior sclera. Additionally, whereas previous studies predominantly focused on the peripapillary region, our study encompassed a broader 9 × 9 mm^2 area

Investigative Ophthalmology & Visual Science

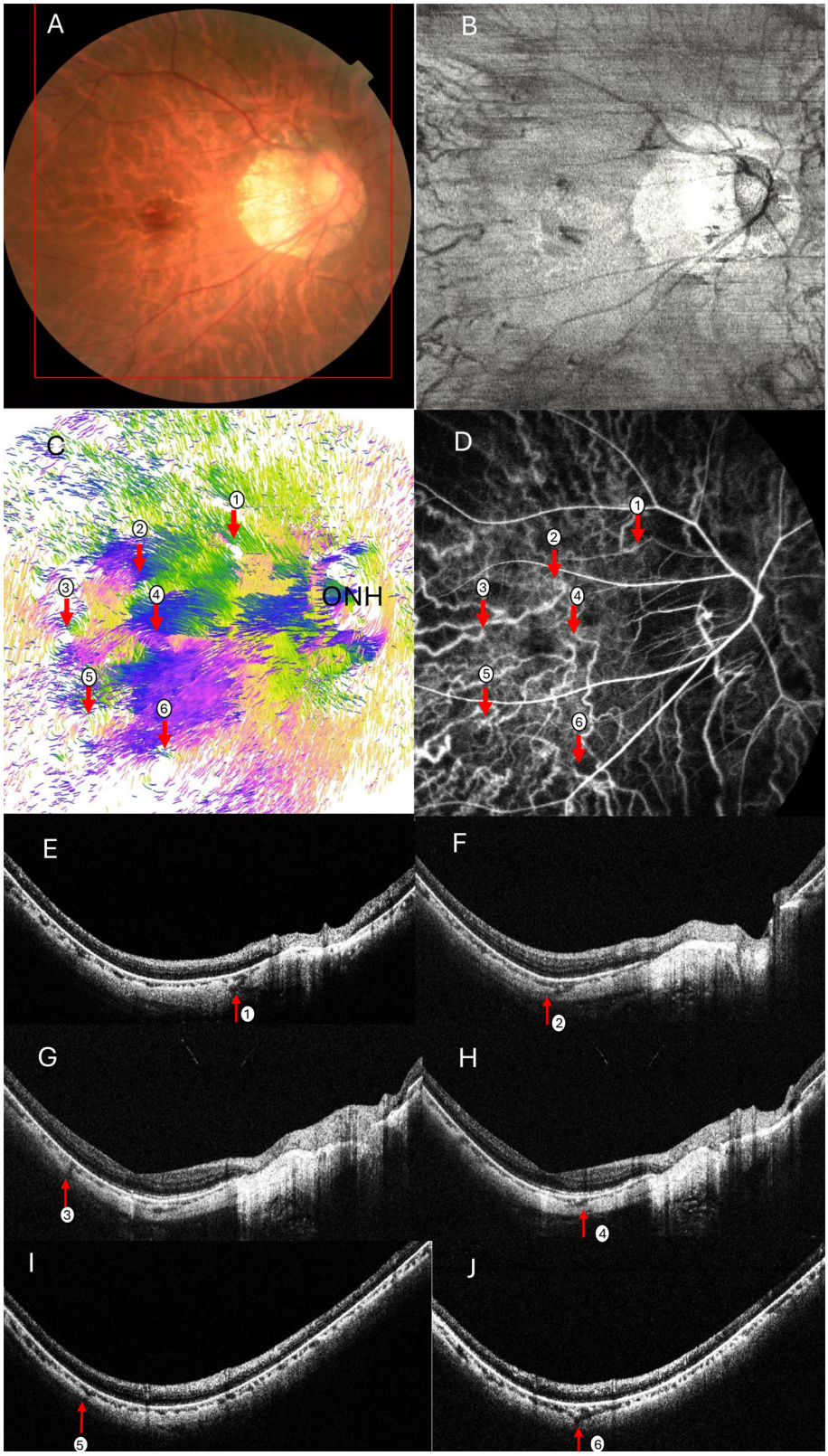

Figure 4. Correspondence of whorl-like structures and emissary canals of PCAs verified by both B-scan OCT intensity images and ICGA scans. **(A)** Right fundus of a 54-year-old highly myopic woman with an axial length of 30.63 mm shows diffuse choroidal atrophy around the optic nerve. The *red rectangle* indicates the capture area of image **B**. **(B)** The en face OCT intensity image of the sclera under CSI. **(C)** The en face streamline cutaway (20 pixels (89.4 µm) below CSI image. *Red arrows* indicate the whorl-like structures. The *arrows* and *numbers* match with those on image **D**. **(D)** Arterial phase ICGA image cropped to the same area as in **B** using the retinal vessels as landmarks. *Arrows* indicate the point where PCAs entered the eye. The whorl-like structures on image **C** all corresponded to PCA emissaries on the ICGA image. **(E–J)** Horizontal B-scan images showing the intrascleral course of PCA (*red arrows*) corresponding to the numbers from 1–6 on images **C** and **D**.

Investigative Ophthalmology & Visual Science

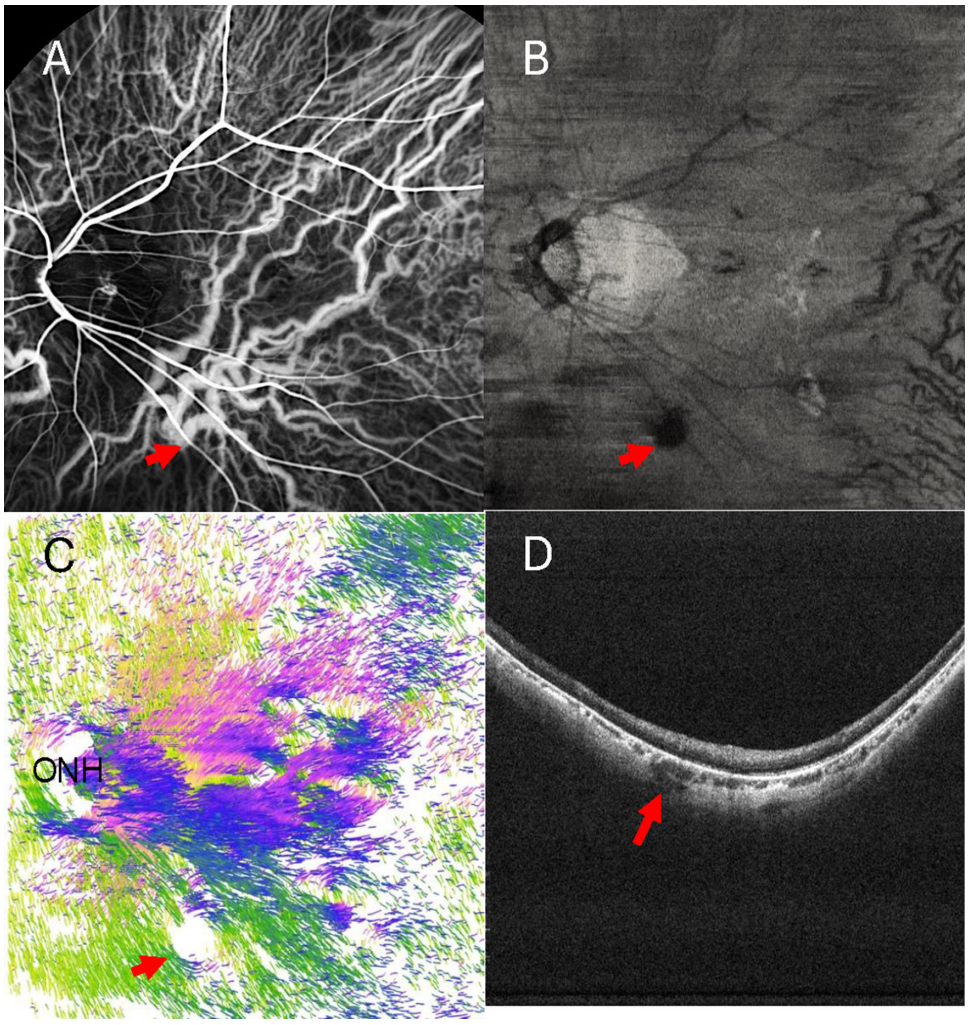

Figure 5. A whorl-like structure surrounding the exit of the posterior VV. **(A)** Venous phase ICGA image from a 54-year-old woman with an axial length of 30.02 mm shows a posterior VV with dilated and tortuous branches. The original ICGA image was cropped to show the area detected by PS-OCT. The *red arrow* indicates the exit of a large posterior VV. **(B)** The en face OCT intensity image at the CSI. The *red arrow* indicates a large hyporeflective area corresponding to the exit of this posterior VV. **(C)** The streamline image viewed from inside the eye shows a large whorl-like structure (*arrow*) corresponding to the site of posterior VV exit. Many other small whorl-like structures were also seen. **(D)** Horizontal B-scan OCT intensity image showing the largest width of the posterior VV. Posterior VV starts from the choroid and courses intrasclerally (between *dotted lines*). The *red arrow* indicates the site where this posterior VV exits the eye.

centered on the fovea and shed light on the macroscopic observation of fiber arrangement in the wider area of sclera.

The emissary canals of PSVs may be structurally vulnerable because they are full-thickness scleral discontinuities, and this vulnerability becomes more pronounced as the posterior sclera stretches and thins in eyes with pathologic myopia. This process can lead to a marked expansion of the canals into scleral pits.[23,24,27] However, previous studies had not thoroughly explored the collagen fiber arrangements around vessel emissary canals within the sclera. In the book *The Sclera*,[1] it is mentioned that "The fibrils at the emissary canals run parallel to the direction of the canal"; however, this assertion lacks supporting citations or illustrative figures and does not provide a clear picture of how the fibrils are arranged around the emissary canals. Our findings contribute to a more detailed understanding of this anatomical configuration, presenting a clearer and more accurate depiction of the collagen fiber orientations in relation to the emissary canals. The whorl-like structures formed by fibers encircling the canals may contribute to maintaining a uniform stress distribution circumferentially, thereby minimizing the risk of stress concentration at any single point. This structural arrangement likely serves a protective role, preserving the space required for vessel passage and preventing potential rupture or significant deformation in these regions under conditions of marked scleral stretching. Scleral remodeling during the progression of myopia is characterized by the loss of collagen tissue, a decrease in collagen fibril diameter, and a shift from an interwoven to a lamellar arrangement of collagen fiber bundles.[28–32] These changes collectively contribute to the overall thinning of the scleral thickness. In the present study, we demonstrated that the whorl-like collagen fiber arrangements appear to remain largely unaffected during this remodeling process. Future ex vivo studies are needed to further investigate the associated microstructural changes.

Investigative Ophthalmology & Visual Science

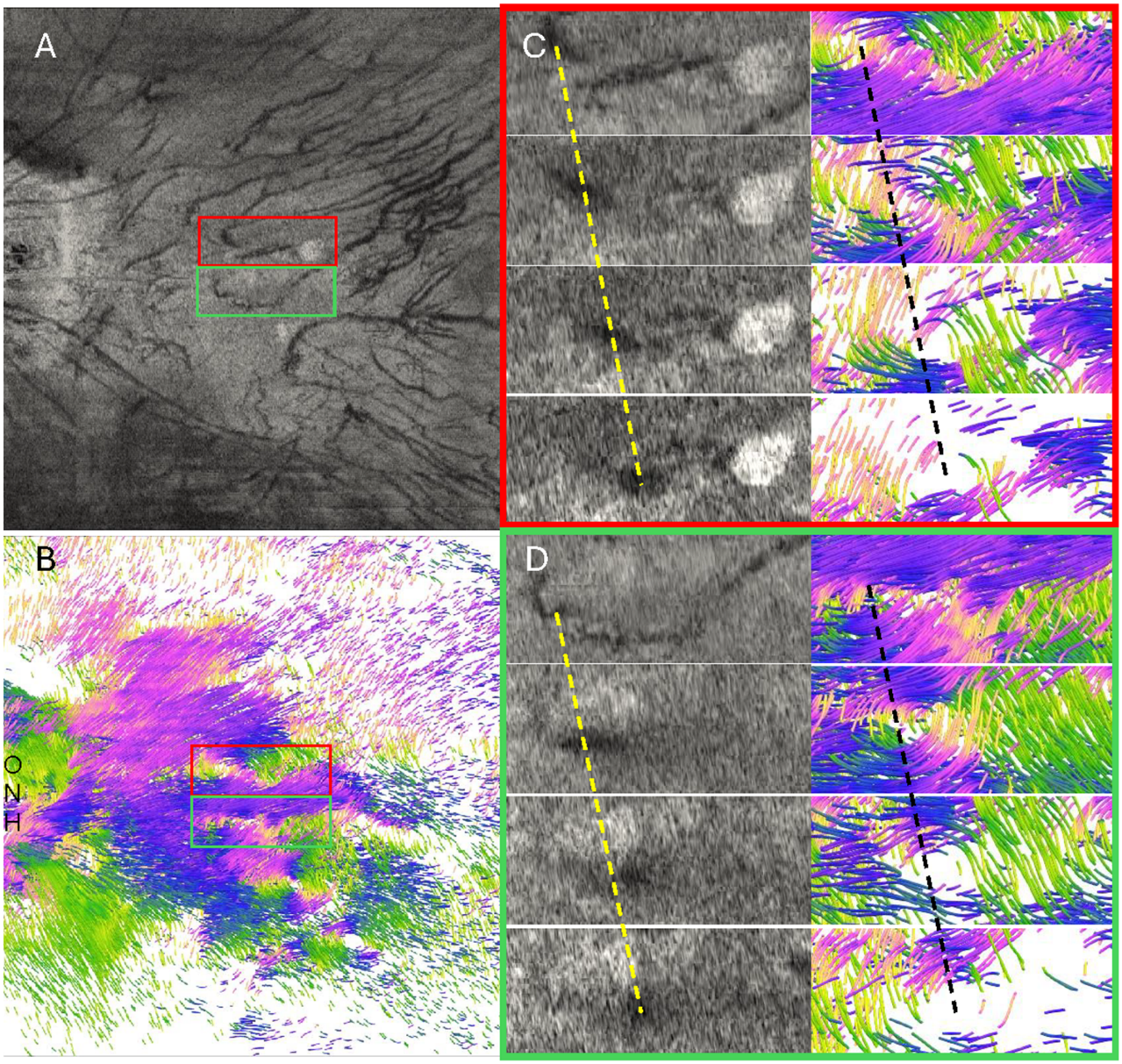

Figure 6. The whorl-like structures observed to encircle the entire course of the emissary canals with the oblique perforation. **(A, B)** En face OCT intensity image at CSI and streamline images of the sclera. The *red* and *green rectangles* indicate the areas shown in images **C** and **D**, respectively. **(C, D)** The cropped images from the areas of **A** and **B** indicated by the *red rectangle* **(C)** and *green rectangle* **(D)**, respectively. The left column in each image shows the en face OCT intensity images extracted at the depths shifted from the CSI for 0 pixel, 10 pixels (44.7 µm), 20 pixels (89.4 µm), and 30 pixels (134.1 µm), respectively. The right column in each image shows the streamline images at the same depths of the respective intensity images in the left column. The *yellow dotted lines* connect the center of the hyporeflective areas, which are indicative of the course of emissary canals, at the depths shifted from CSI for 0 and 30 pixels. It can be observed that both emissary canals are oblique within the sclera, because they perforate the sclera temporally and inferiorly from CSI to deeper levels. The *black dotted lines* connect the center of the whorl-like structures at the depths shifted from CSI for 0 and 30 pixels, showing corresponding lateral shift along the depths in the sclera, as well as the OCT intensity images.

Additionally, tangentially arranged collagen bundles were observed around the emissary canals under microscopy. Similar tangentially arranged fibers have also been reported to surround the ONH canal in a study by Voorhees and colleagues,[33] they pointed out that the tangentially arranged fiber might explain the expansion of the ONH canal under elevated intraocular pressure. Moreover, they performed computational modeling and demonstrated that tangentially arranged fibers showed significantly superior profile of circumferential and radial strains compared to traditional circumferential fiber arrangement and radial fiber arrangement models.[33] Therefore the tangentially arranged fibers, which provide flexibility of expansion and near-zero strain profile,[33] might be a more deep-seated factor for the mechanical strength of such whorl-like configuration, especially in cases of scleral pits. The persistence of whorl-like structures around scleral pits, hypothesized to arise from the expansion of tangentially arranged fibers, further supports the role of collagen fiber sliding as a biomechanical mechanism contributing to ocular expansion in myopic eyes.[34]

Investigative Ophthalmology & Visual Science

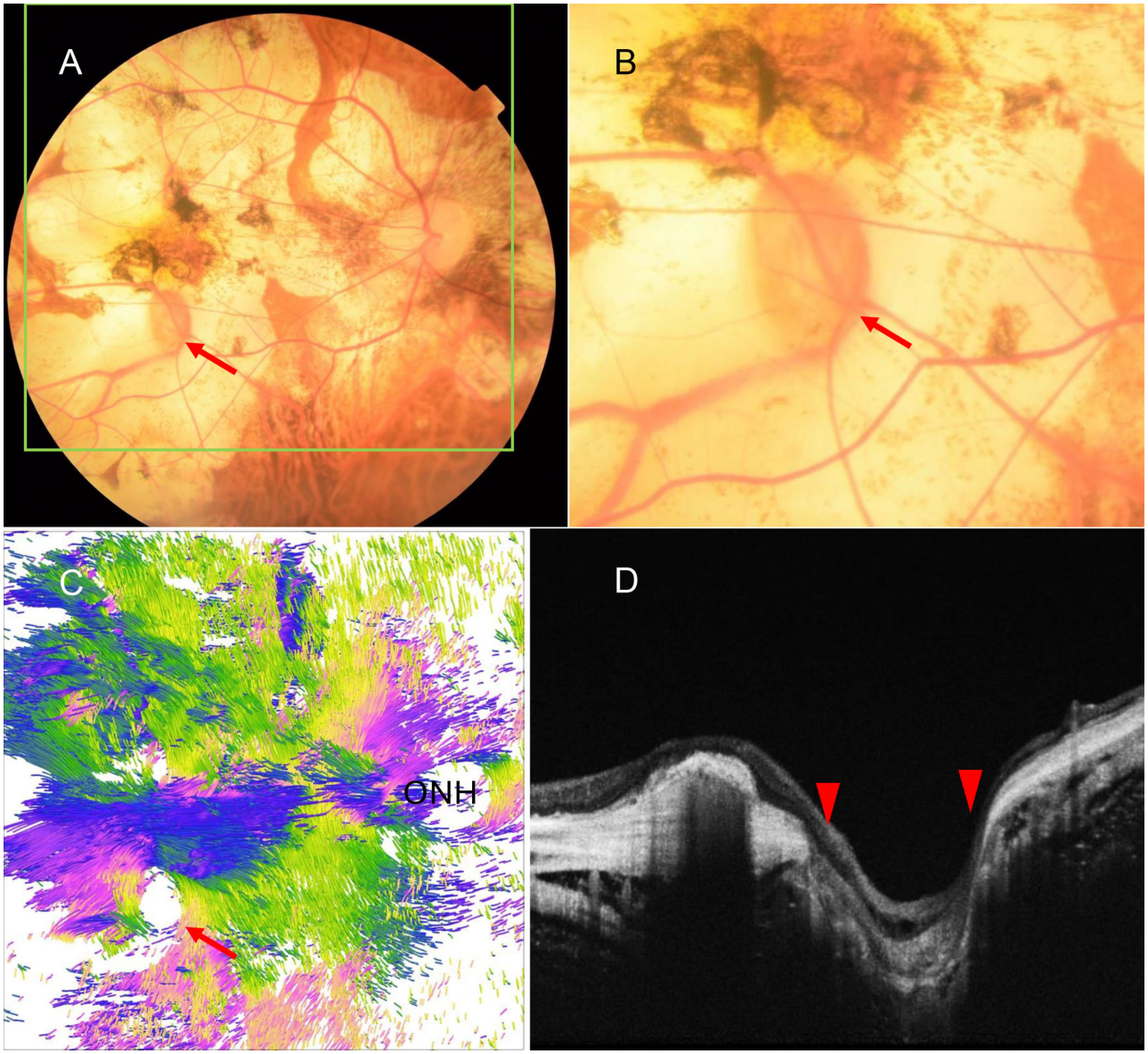

Figure 7. A case with whorl-like structure surrounding a large scleral pit. **(A)** Left fundus of a 59-year-old woman with an axial length of 32.64 mm shows extensive atrophy. The *red arrow* indicates the scleral pit with slightly orange color. **(B)** A magnified image of the scleral pit. Branches of the perforating scleral vessel emerges at the edge of the pit. **(C)** Streamline image of the sclera. The *red arrow* indicates a large whorl-like structure corresponding to the pit area. **(D)** A vertical scan of swept-source OCT (SS-OCT) at the pit area shows that the sclera is disrupted at the point indicated by *arrowheads*. The width of the pit is 896.48 µm.

Scleral pits are larger full-thickness scleral excavation occurring at the site of emissary canals in advanced pathologically myopic eyes with extensive choroid atrophy, which are believed to be caused by a mechanical expansion of the emissary canals as a result of axial elongation, scleral thinning and loss of overlying choroid.[23,24,27] It has been reported to occur in 17.6% to 59% of pathologically myopic eyes.[19,20] In our study, the largest widths measured ranged from 150 to 900 µm, while a previous small case series[35] reported scleral pit sizes ranging from 0.5 to 1 disc diameter (approximately 1500 µm). Both findings indicate a relatively large scleral hole on a very thin sclera. Therefore it is conceivable that these areas would be extremely vulnerable, and the whorl-like structures around scleral pits demonstrated by PS-OCT in our study may provide important insights on how the eyes maintain integrate in such cases, and no spontaneous eye rupture occurred in such cases in our Advanced High Myopia Center.

Additionally, when scleral pits are present, the vessels are consistently located at the edge of the pits rather than at their center in color fundus photographs (Fig. 7).[23,24,27] Under SEM examination of porcine eyes, vessels were observed to be firmly attached to one side of the emissary canal eccentrically, with many accompanying connective tissues (Fig. 8C). This anatomical structure may explain the abovementioned clinical findings.

This study has several limitations that must be acknowledged. First, it focuses exclusively on highly myopic eyes, which could exhibit different patterns of collagen fiber arrangements from those in normal human eyes. However,

Investigative Ophthalmology & Visual Science

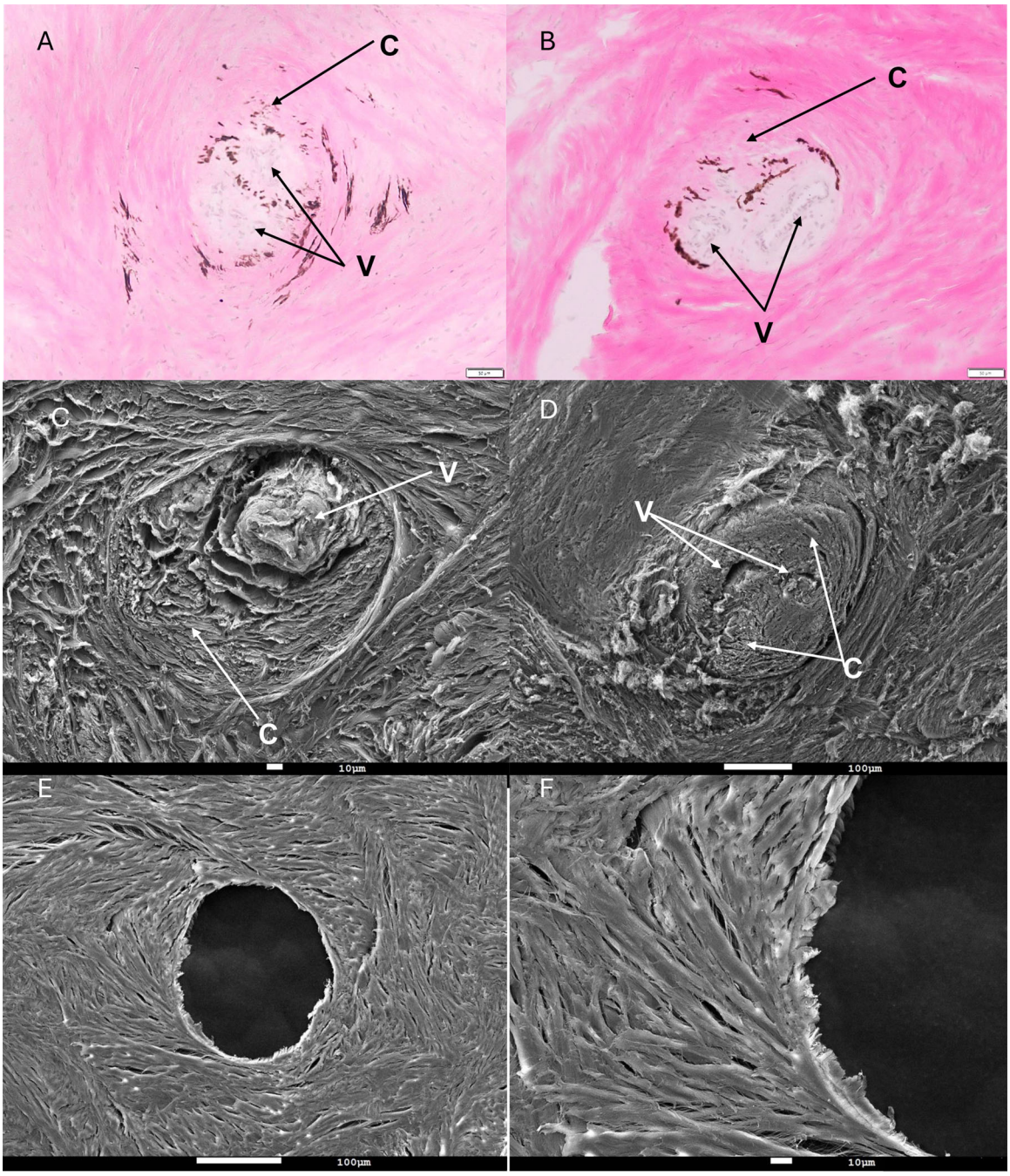

Figure 8. The arrangement of collagen fibers around the emissary canals in the posterior sclera of a porcine eye was examined using microscopy techniques. **(A, B)** Light microscopic images of H&E-stained 10 µm-thick scleral sections reveal a circumferential organization of collagen fibers encircling the emissary canals. Multiple vessels (*V*) are visible within a single canal, accompanied by surrounding collagen fibers (*C*). Magnification ×200. *Scale bars*: 50 µm. **(C, D)** SEM images display one **(C)** or two **(D)** vessels (*V*) within the emissary canals, accompanied by collagen fibers (*C*). Collagen fibers around the emissary canals are arranged circumferentially. **(C)** A vessel is positioned eccentrically, attaching to one side of the canal. Magnification ×370 for **C** (*Scale bar*: 10 µm) and ×160 for **D** (*Scale bar*: 100 µm). **(E)** SEM image of a 10 µm thick slice displaying an emissary canal without vessels inside. Magnification ×200. *Scale bar*: 100 µm. **(F)** Close-up of the lower left part of the emissary canal from image **E**, showing collagen fibers arranged tangentially around the canal. Magnification ×500. *Scale bar*: 10 µm.

by microscopic observation of porcine sclera, which shares many structural similarities with human sclera and is widely used as a model for studying ocular biomechanics,[36] we confirmed that this configuration is a normal structure. Second, the detailed structures of the sclera,[20] including the hierarchical organization of collagen (from tropocollagen molecules to microfibrils and fibrils), the crimp structures of the fibers, and the variation in fiber and bundle diameters across different scleral depths, exceed the resolution of PS-OCT, and the streamline images represent only the preferential collagen fiber orientations based on the net birefringence detected by the device. Future ex vivo studies are

Investigative Ophthalmology & Visual Science

needed to further investigate the associated microstructural changes around emissary canals in myopic eyes.

In conclusion, our study demonstrated the presence of whorl-like structures constructed by tangentially arranged collagen fibers around PSV emissary canals in the posterior sclera using PS-OCT in vivo and microscopy ex vivo, thereby addressing a previously unexplored aspect of scleral histology. The whorl-like structures around large scleral pits highlighted the critical role of this configuration in the structural integrity and physiological function of the eye in extremely pathological conditions. These findings not only fill a significant knowledge gap but also opens avenues for further research into the biomechanical properties of the sclera and their implications for ocular health. Further longitudinal istudies using PS-OCT for highly myopic eyes might be able to detect early changes of the sclera at structurally vulnerable sites that predispose the patients to significant morphological changes like deep staphyloma before developing vision-threatening complications.

Acknowledgments

Supported by partial research funding from Tomey Corporation. Grant from the Japanese Society for Promotion of Science (number; 19H03808) to K.O.M, and grant from JST SPRING, Grant Number JPMJSP2120 to H. L.

Disclosure: **H. Lu**, None; **Y. Wu**, None; **J. Xiong**, None; **N. Zhou**, None; **M. Yamanari**, Tomey Corporation (E), JP 6463051 B2 (P), US 9593936 B2 (P), EP 2995245 B1 (P), JP 6542178 B2 (P), JP 7332131 B2 (P) issued to Tomey Corporation; **M. Okamoto**, Tomey Corporation (E); **K. Sugisawa**, None; **H. Takahashi**, None; **C. Chen**, None; **Y. Wang**, None; **Z. Wang**, None; **K. Ohno-Matsui**, Tomey Corporation (R), Santen (C), CooperVision (C)

References

1. Stanford M. The sclera, M. S. De La Maza, J. Tauber, C. S. Foster 2013, ISBN: 978-1-4419-6501-1 Springer [book review]. *Graefes Arch Clin Exp Ophthalmol*. 2014;252:2027.
2. Watson PG, Young RD. Scleral structure, organisation and disease. A review. *Exp Eye Res*. 2004;78:609–623.
3. Meek KM. The cornea and sclera. In: Fratzl P, ed. *Collagen: Structure and Mechanics*. Boston: Springer US; 2008:359–396.
4. Hayreh SS. Posterior ciliary artery circulation in health and disease: the Weisenfeld lecture. *Invest Ophthalmol Vis Sci*. 2004;45:749–757; 748.
5. Moriyama M, Cao K, Ogata S, Ohno-Matsui K. Detection of posterior vortex veins in eyes with pathologic myopia by ultra-widefield indocyanine green angiography. *Br J Ophthalmol*. 2017;101:1179–1184.
6. He G, Zhang X, Zhuang X, et al. A novel exploration of the choroidal vortex vein system: incidence and characteristics of posterior vortex veins in healthy eyes. *Invest Ophthalmol Vis Sci*. 2024;65(2):21.
7. Willemse J, Gräfe MGO, Verbraak FD, de Boer JF. In vivo 3D determination of peripapillary scleral and retinal layer architecture using polarization-sensitive optical coherence tomography. *Transl Vis Sci Technol*. 2020;9(11):21.
8. Ohno-Matsui K, Igarashi-Yokoi T, Azuma T, et al. Polarization-sensitive OCT imaging of scleral abnormalities in eyes with high myopia and dome-shaped macula. *JAMA Ophthalmol*. 2024;142:310–319.
9. Komai Y, Ushiki T. The three-dimensional organization of collagen fibrils in the human cornea and sclera. *Invest Ophthalmol Vis Sci*. 1991;32:2244–2258.
10. Jan N-J, Lathrop K, Sigal IA. Collagen architecture of the posterior pole: high-resolution wide field of view visualization and analysis using polarized light microscopy. *Invest Ophthalmol Vis Sci*. 2017;58:735–744.
11. Gogola A, Jan NJ, Lathrop KL, Sigal IA. Radial and circumferential collagen fibers are a feature of the peripapillary sclera of human, monkey, pig, cow, goat, and sheep. *Invest Ophthalmol Vis Sci*. 2018;59:4763–4774.
12. Zhang L, Albon J, Jones H, et al. Collagen microstructural factors influencing optic nerve head biomechanics. *Invest Ophthalmol Vis Sci*. 2015;56:2031–2042.
13. Hecht E. *Optics*. New York: Pearson Education, Inc.; 2017.
14. Patil R, Shetty R, Patel Y, et al. Phase retardation and corneal sublayer thickness repeatability using ultrahigh-resolution polarization-sensitive OCT. *J Cataract Refract Surg*. 2023;49:76–83.
15. Patil R, Shetty R, Narasimhan R, et al. Mapping of corneal birefringence in thin and asymmetric keratoconus corneas with ultrahigh-resolution polarization-sensitive OCT. *J Cataract Refract Surg*. 2022;48:929–936.
16. Steiner S, Schwarzhans F, Desissaire S, et al. Birefringent properties of the peripapillary retinal nerve fiber layer in healthy and glaucoma subjects analyzed by polarization-sensitive OCT. *Invest Ophthalmol Vis Sci*. 2022;63(12):8.
17. Gräfe MGO, van de Kreeke JA, Willemse J, et al. Subretinal fibrosis detection using polarization sensitive optical coherence tomography. *Transl Vis Sci Technol*. 2020;9(4):13.
18. Yamanari M, Mase M, Obata R, et al. Melanin concentration and depolarization metrics measurement by polarization-sensitive optical coherence tomography. *Sci Rep*. 2020;10(1):19513.
19. Li Q, Karnowski K, Untracht G, et al. Vectorial birefringence imaging by optical coherence microscopy for assessing fibrillar microstructures in the cornea and limbus. *Biomed Opt Express*. 2020;11:1122–1138.
20. Boote C, Sigal IA, Grytz R, Hua Y, Nguyen TD, Girard MJA. Scleral structure and biomechanics. *Prog Retin Eye Res*. 2020;74:100773.
21. Pijanka JK, Spang MT, Sorensen T, et al. Depth-Dependent Changes in Collagen Organization in the Human Peripapillary Sclera. *PLoS ONE*. 2015;10(2):e0118648.
22. Ohno-Matsui K, Akiba M, Ishibashi T, Moriyama M. Observations of vascular structures within and posterior to sclera in eyes with pathologic myopia by swept-source optical coherence tomography. *Invest Ophthalmol Vis Sci*. 2012;53:7290–7298.
23. Xie S, Fang Y, Du R, et al. Abruptly emerging vessels in eyes with myopic patchy chorioretinal atrophy. *Retina*. 2019;40:1.
24. Pedinielli A, Souied EH, Perrenoud F, Leveziel N, Caillaux V, Querques G. In Vivo visualization of perforating vessels and focal scleral ectasia in pathological myopia. *Invest Ophthalmol Vis Sci*. 2013;54:7637–7643.
25. Ohno-Matsui K, Kawasaki R, Jonas JB, et al. International photographic classification and grading system for myopic maculopathy. *Am J Ophthalmol*. 2015;159:877–883.e877.
26. Liu X, Jiang L, Ke M, et al. Posterior scleral birefringence measured by triple-input polarization-sensitive imaging as a biomarker of myopia progression. *Nat Biomed Eng*. 2023;7:986–1000.
27. Ohno-Matsui K, Akiba M, Moriyama M. Macular pits and scleral dehiscence in highly myopic eyes with macular chorioretinal atrophy. *Retin Cases Brief Rep*. 2013;7:334–337.
28. Liu KR, Chen MS, Ko LS. Electron microscopic studies of the scleral collagen fiber in excessively high myopia. *Taiwan Yi Xue Hui Za Zhi*. 1986;85:1032–1038.
29. Curtin BJ, Iwamoto T, Renaldo DP. Normal and staphylomatous sclera of high myopia: an electron microscopic study. *Arch Ophthalmol*. 1979;97:912–915.

30. McBrien NA, Cornell LM, Gentle A. Structural and ultrastructural changes to the sclera in a mammalian model of high myopia. *Invest Ophthalmol Vis Sci*. 2001;42:2179–2187.
31. Funata M, Tokoro T. Scleral change in experimentally myopic monkeys. *Graefes Arch Clin Exp Ophthalmol*. 1990;228:174–179.
32. McBrien NA, Gentle A. Role of the sclera in the development and pathological complications of myopia. *Prog Retin Eye Res*. 2003;22:307–338.
33. Voorhees AP, Jan N-J, Hua Y, Yang B, Sigal IA. Peripapillary sclera architecture revisited: a tangential fiber model and its biomechanical implications. *Acta Biomaterialia*. 2018;79:113–122.
34. Rada JA, Shelton S, Norton TT. The sclera and myopia. *Exp Eye Res*. 2006;82:185–200.
35. Zhang W, Zhang Y, Xu J, Dan H, Li X, Song Z. A physical sign of pathological myopia: myopic scleral pit. *BMC Ophthalmol*. 2023;23:114.
36. Herring I, Duncan R, Pickett J, Bass C. The porcine eye as a surrogate model for the human eye: anatomical and mechanical relationships. Available at https://www-nrd.nhtsa.dot.gov⟩bio⟩Proceedings. Accessed October 24, 2024.

Supplementary Material

Supplementary Video. Video showing *en face* optical coherence tomography (OCT) intensity and streamline images of the sclera extracted at the shifted depths from the choroid-sclera interface (CSI) for 0 to 31 pixels (138.6 µm). From CSI to deeper levels, the positions of the emissary canals indicated by hypo-reflective area on the intensity images shift laterally, and the respective whorl-like structures on the corresponding streamline images shift accordingly at each depth.

Investigative Ophthalmology & Visual Science